SAND2016-1722C

Tailoring Dielectric Resonator Geometries for Directional Scattering, Huygens' Metasurfaces, and High Quality-Factor Fano Resonances

Salvatore Campione[*,†], Lorena I. Basilio[*], Larry K. Warne[*], William L. Langston[*], Ting S. Luk[*,†], Joel R. Wendt[*], Sheng Liu[*,†], Igal Brener[*,†], and Michael B. Sinclair[*]

[*]Sandia National Laboratories, P.O. Box 5800 Albuquerque, NM 87185 USA
[†]Center for Integrated Nanotechnologies, Sandia National Laboratories, P.O. Box 5800 Albuquerque, NM 87185 USA
e-mail: sncampi@sandia.gov

***Abstract*—Metamaterial dielectric resonators represent a promising path toward low-loss metamaterials at optical frequencies. In this paper we utilize perturbations of high symmetry resonator geometries, such as cubes, either to overlap the electric and magnetic dipole resonances, thereby enabling directional scattering and Huygens' metasurfaces, or to induce couplings between the otherwise orthogonal resonator modes to achieve high-quality factor Fano resonances. Our results are fully scalable across any frequency bands where high-permittivity dielectric materials are available, including microwave, THz, and infrared frequencies.**

I. Introduction

High intrinsic Ohmic losses exhibited by metallic resonators limit their applicability to resonant metamaterials operating at infrared and higher frequencies. A promising alternative building block is represented by dielectric resonators (DRs), which could be used to develop low-loss resonant metamaterials. The reason for this is that lossy Ohmic currents of metallic resonators become substituted for low-loss displacement currents in DRs.

However, the use of DRs is not without its own challenges: achieving the desired resonant properties while maintaining a sufficiently small resonator size and spacing requires the use of very high permittivity materials. At THz and microwave frequencies, permittivity values larger than 100 are readily available. In contrast, at infrared wavelengths, the largest permittivity available is approximately 32 (for example, for lead telluride). In this way, designing the geometric details of the DR and assembling them into metamaterials, while still maintaining effective medium behavior is challenging; yet, as will be shown in this paper, it is possible.

In this paper, we will make use of perturbations [1-3] of high symmetry DR geometries, such as cubes and spheres, either to overlap the electric and magnetic dipole resonances, thereby enabling directional scattering [3-6] and Huygens' metasurfaces [3, 7, 8], or to induce couplings between the otherwise orthogonal resonator modes to achieve high-quality factor Fano resonances. Both directions open up new avenues towards practical applications of all-dielectric metasurfaces, including ultra-lightweight flat optics such as lensing and wave-front manipulation with Huygens' metasurfaces [9]. Importantly, this approach is frequency scalable and could be used from microwave to near-infrared frequencies.

II. Directional Scattering and Huygens' Metasurfaces

The use of perturbation techniques [1, 2] can lead to DR geometries that selectively adjust the spectral locations of the resonances. Split-cubes or split-spheres were the suggested designs to overlap the electric and magnetic dipole resonances in the same frequency band. For example, to shift the magnetic resonance frequency upwards towards the electric resonance frequency, the splits should be arranged in such a manner as to selectively interact with the electric field pattern of the magnetic resonance and leave the electric resonance unaffected.

In this paper, as shown in the insets of Fig. 1, we consider a DR cube containing a split in the midplane transverse to the plane wave propagation direction, creating a small gap between the two half cubes. We analyze two values of the gap, namely 100 and 200 nm, to show that the perturbation causes the magnetic dipole resonance to move towards the electric dipole resonance. For simplicity, we describe the electric and magnetic dipole moments in terms of electric and magnetic dipole polarizability tensors [10]:

$$\mathbf{p} = \underline{\boldsymbol{\alpha}}_{\mathrm{ee}} \cdot \mathbf{E}_{\mathrm{loc}}, \quad \mathbf{m} = \underline{\boldsymbol{\alpha}}_{\mathrm{mm}} \cdot \mathbf{H}_{\mathrm{loc}} \tag{1}$$

where $\underline{\boldsymbol{\alpha}}_{\mathrm{ee}}$ and $\underline{\boldsymbol{\alpha}}_{\mathrm{mm}}$ are the electric and magnetic dipole polarizability tensors and $\mathbf{E}_{\mathrm{loc}}$ and $\mathbf{H}_{\mathrm{loc}}$ are the local electric and magnetic fields acting on the resonator. The polarizability tensors will be diagonal with equal components for isotropic resonators. The split cubes will exhibit diagonal polarizability tensors, however some components will be different from each other. For this reason, we show only the transverse components, here marked as α_{ee} and α_{mm}.

Using full-wave simulations [3, 11, 12], we estimate the electric and magnetic dipole polarizabilities of full cubes and split cubes. Figure 1 shows the electric and magnetic polarizabilities for a full cube as well as split cubes with two different gap widths as shown in the insets.

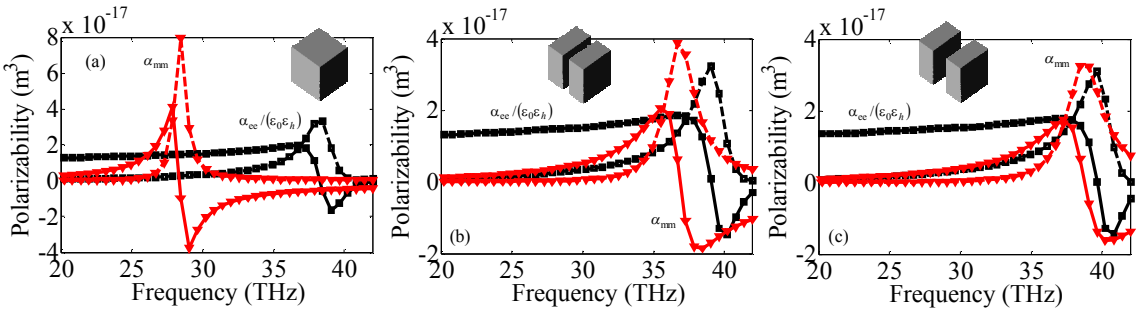

Fig. 1. The frequency location of DRs' electric and magnetic polarizabilities is controllable through geometry. Solid: Real part; dashed: imaginary part. (a) Full-cube. (b) Split-cube with gap = 100 nm. (c) Split-cube with gap = 200 nm. The monochromatic time harmonic convention $\exp(-i\omega t)$ is assumed.

This figure presents polarizabilities in units of m^3, i.e. the electric polarizability in Eq. (1) has been normalized to the host absolute permittivity $\varepsilon_0\varepsilon_h$. First, let's analyze the results for the full cube: we observe a magnetic dipole resonance (red triangles) around 28.31 THz followed by an electric dipole resonance (black squares) around 38.37 THz. Then, let's understand the effect of introducing a gap in the split cubes: it is evident such gap causes the magnetic resonance to move toward higher frequencies (red triangles), while leaving the frequency location of the electric resonance frequency almost unaffected (black squares). In particular, for the 200 nm split cube of Fig. 1(c), the magnetic dipole resonance (38.97 THz) is nearly overlapped with the electric dipole resonance (39.47 THz). This is an interesting effect that we will investigate in what follows for the purpose of directional scattering and Huygens' metasurfaces.

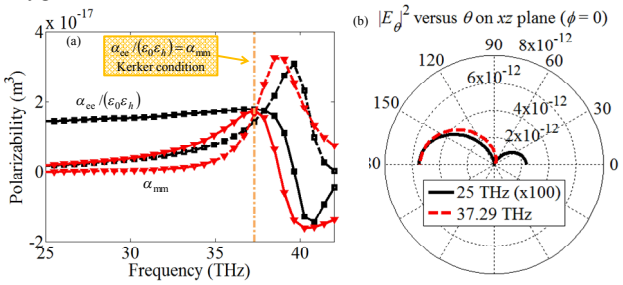

Fig. 2. (a) Polarizability result shown in Fig. 1(c), where we mark a frequency that satisfies the first Kerker condition with the dashed-dotted vertical line. (b) Scattered radiation pattern of an isolated split cube resonator excited through plane wave incidence for two excitation frequencies, 25 and 37.29 THz. Forward scattering is evident (i.e. only one lobe at $\theta = 180$ degrees) when the first Kerker condition is satisfied. Only data between 0 and 180 degrees is reported; the scattering is specular between 180 and 360 degrees.

An appropriate overlap of electric and magnetic resonances may lead to directional forward or backward scattering for isolated resonators [4-6]. In particular, the first Kerker condition [4, 5] states that an isolated resonator will predominantly scatter light in the forward direction when $a_1 = b_1$, with a_1 and b_1 the Mie electric and magnetic dipole coefficients. Furthermore, a_1 and b_1 should be significantly larger than any higher order Mie terms $a_n, b_n : n > 1$. Since $\alpha_{ee}/(\varepsilon_0\varepsilon_h) = 6\pi i a_1/k^3$ and $\alpha_{mm} = 6\pi i b_1/k^3$, we can equivalently express these conditions through the electric and magnetic dipole polarizabilities defined earlier as $\alpha_{ee}/(\varepsilon_0\varepsilon_h) = \alpha_{mm}$. Interestingly, we observe in Fig. 2(a) that this condition is (almost perfectly) satisfied for both real and imaginary components of the polarizabilities near 37.29 THz (indicated by the vertical dashed-dotted orange line). The scattered radiation pattern of an isolated split cube resonator (gap of 200 nm) excited through plane wave incidence is shown in Fig. 2(b) for two excitation frequencies: 25 and 37.29 THz. A single-lobed radiation pattern – a signature of forward scattering – is obtained at the frequency that satisfies the Kerker condition (37.29 THz). In contrast, a weaker, two-lobed scattering pattern is observed at the nonresonant frequency of 25 THz for which the Kerker condition is not satisfied. We envision that, by further tailoring the resonator design to better overlap the spectral position, width, and amplitude of the two polarizabilities, it may be possible to satisfy the Kerker conditions over a frequency band, rather than at isolated frequencies.

To assess the applicability of these resonator geometries to metamaterials, consider a two-dimensional array of resonators arranged on a square lattice with a period of 2.6 μm. We employ the resonator geometries of Fig. 1(a) (full cube) and Fig. 1(c) (single-split cube with 200 nm gap). The reflectance and transmittance under normal plane wave incidence of such arrays are shown in Figs. 3(a)-3(b). Profound differences are observed between the spectra obtained for the two geometries. The array of full dielectric cubes (which possess electric and magnetic dipole resonances at separate frequencies) exhibits two strong reflection maxima and two corresponding transmission minima. In contrast, the array of split-cubes is highly transmissive over a wide frequency band because of the near overlap of dipolar resonances as shown in Fig. 1(c). We also report the phases of the reflection and transmission coefficients at a distance of 8 μm from the array plane in Figs. 3(c)-3(d) for the two arrays here considered. In agreement with [7], the transmission coefficient for the full cube metamaterial undergoes a phase shift of at most 180 degrees at each resonance, while the transmission coefficient for the split-cube metamaterial

undergoes a complete 360 degree phase shift. This combination of features — high transmittance and 360 degree phase shift — renders the split-cube metamaterial design appealing for use in Huygens' metasurfaces [7] which are a promising platform for the development of flat optical devices. We further note that the reflection behavior is opposite than that of the transmission: high reflectivity across a broad spectral range and a full 360 degree phase shift are only obtained for the full cube metamaterial. Thus, the full cube metamaterial allows us to manipulate the reflection response and realize a metareflector that can be very easily fabricated. These fundamental differences between the behaviors of the two metamaterials demonstrate the dramatic impact that perturbations at the single resonator level can have on the metamaterial performance at the macroscopic level.

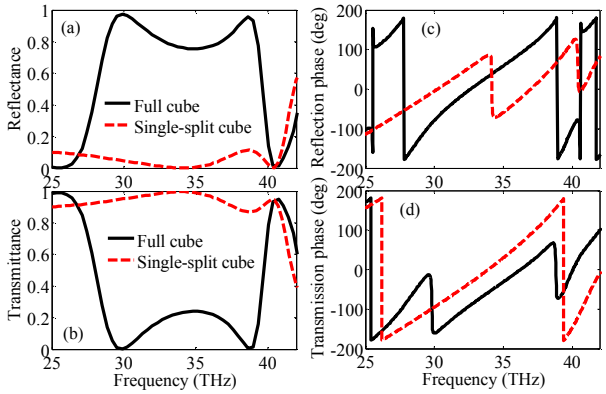

Fig. 3. (a) Reflectance and (b) transmittance of a two-dimensional array of full cubes as in Fig. 1(a) and split cubes as in Fig. 1(c) arrayed on a square lattice with a period of 2.6 μm. Phase of the (c) reflection and of the (d) transmission coefficient for the cases in (a)-(b).

III. High-Quality Factor FAno Resonances

In this section, our goal is to develop a perturbed resonator design that allows us to obtain high-quality factor Fano resonances. A common feature of the DR-based Fano designs demonstrated so far is the reliance on multiple, distinct, near-field coupled dielectric structures within the unit cell [13-15]. However, reliable and repeatable control of near-field coupling requires exacting fabrication tolerances. It is therefore of interest to inquire if simpler high quality-factor Fano designs can be developed. Here, we demonstrate a monolithic DR design that achieves ultra-high quality-factors while using only one dielectric structure per unit cell. Our approach relies on intra-resonator mixing of bright and dark modes, and is scalable from radio frequencies to near-infrared frequencies.

The resonator design starts with a simple cubic resonator similar to the dielectric resonators demonstrated in Fig. 1(a). Such a high-symmetry geometry leads to orthogonal, but degenerate, sets of electric and magnetic dipole modes oriented along the *x*-, *y*-, and *z*-directions (along with other higher order multipoles). When arranged in a subwavelength metasurface, only the transverse (i.e. in-plane) dipole modes can couple to a normal external wave and this results in the usual electric and magnetic transmission/reflection resonances in Fig. 3. However, it is possible to perturb the geometry to induce mode mixing between the transverse electric and longitudinal magnetic dipole modes. A schematic design of the proposed perturbed DR design based upon germanium is shown in Fig. 4(a). Starting with a cubic geometry, a notch has been cut from one corner of the cube, and the adjacent corner has been slightly extended. Full-wave simulation of the scattering from an isolated resonator reveals that under electric field excitation conditions with the incident *E*-field in the *x*-direction, the out-of-plane (i.e. *z*-directed) magnetic dipole is strongly excited near 10.7 μm. This occurs indirectly, through coupling to the *x*-directed electric dipole. For an isolated resonator, the *z*-directed dipole is free to radiate, however when placed in a subwavelength metasurface, the dipole's emission is suppressed by the local field [16]. We show in Fig. 4(b) the reflectivity spectrum obtained from full-wave simulation of an array of perturbed Ge resonators on a barium fluoride substrate. Several, extremely narrow Fano resonances are observed — the transmission spectrum (not shown) exhibits complementary (pass-band) transmission resonances. The quality factor of the reflection resonance (as defined by $f_0/\Delta f$ where f_0 is the resonant frequency and Δf is the full width at half minimum of the resonance) at ~ 10.7 μm exceeds 1300.

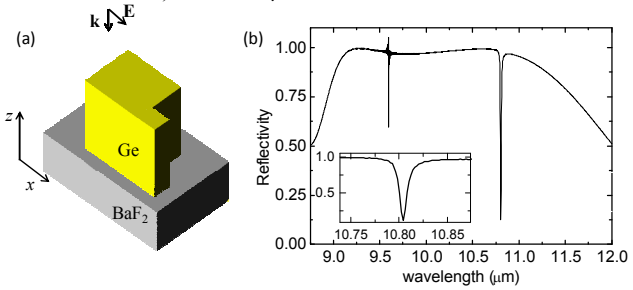

Fig. 4. (a) A schematic of the unit cell of the Fano metasurface design. (b) The numerical reflectivity spectrum of the array. The inset shows a zoomed view of the resonance at ~10.7 μm, whose quality-factor is ~1300.

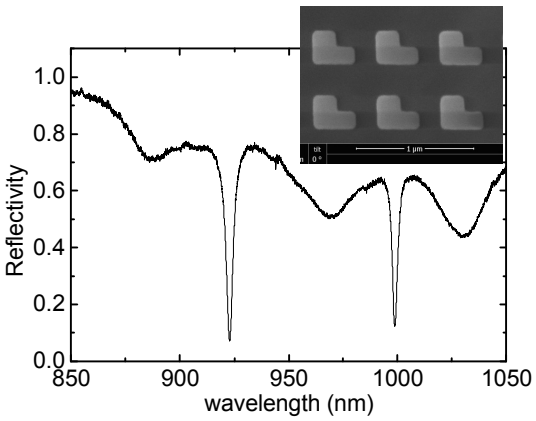

Fig. 5. The experimentally measured reflectivity spectrum of the array in the inset. The quality-factor for the resonance at 999 nm is ~350.

Next, we want to experimentally demonstrate the new Fano design. Thus, we have designed and fabricated silicon-based Fano resonators operating near 1 μm wavelength. We used silicon-on-insulator wafers with a 250 nm thick silicon layer.

The nominal side length of the resonators is 280 nm and the array spacing is 550 nm. We fabricated the arrays using e-beam lithography (the inset of Fig. 5 shows a scanning electron micrograph of several of the resonators in the array). Reflectivity measurements were made using a custom built near-infrared polarizing microscope coupled to a high resolution spectrometer equipped with a CCD array detector. Figure 5 shows the experimentally measured reflectivity spectrum, which features multiple Fano resonances as expected from theory. The measured quality factor of the resonance at 999 nm is about 350, in agreement with theory, confirming that the proposed design is effective for the purpose of obtaining high-quality, pass-band resonances. These resonances could be used to improve the efficiency of sensing devices, for example.

IV. Conclusion

In conclusion, we described a methodology for tailoring the design of metamaterial dielectric resonators by utilizing perturbations of high symmetry resonator geometries, such as cubes or spheres. In this way, we can overlap the electric and magnetic dipole resonances, thereby enabling directional scattering and Huygens' metasurfaces. We can also induce couplings between the otherwise orthogonal resonator electric and magnetic modes to achieve high-quality factor Fano resonances. Our results are fully scalable across any frequency bands where high-permittivity dielectric materials are available, and open up new avenues towards practical applications of all-dielectric metasurfaces.

Acknowledgment

Parts of this work were supported by the U.S. Department of Energy, Office of Basic Energy Sciences, Division of Materials Sciences and Engineering and performed, in part, at the Center for Integrated Nanotechnologies, an Office of Science User Facility operated for the U.S. Department of Energy (DOE) Office of Science. Sandia National Laboratories is a multi-program laboratory managed and operated by Sandia Corporation, a wholly owned subsidiary of Lockheed Martin Corporation, for the U.S. Department of Energy's National Nuclear Security Administration under contract DE-AC04-94AL85000.

References

[1] L. K. Warne, L. I. Basilio, W. L. Langston, W. A. Johnson, and M. B. Sinclair, "Perturbation Theory in the Design of Degenerate Spherical Dielectric Resonators," *IEEE Trans. Antennas Propagat.* , vol. 61, pp. 2130-2141, 2013.

[2] L. K. Warne, L. I. Basilio, W. L. Langston, W. A. Johnson, and M. B. Sinclair, "Perturbation theory in the design of degenerate rectangular dielectric resonators," *Progress In Electromagnetics Research B,* vol. 44, pp. 1-29, 2012.

[3] S. Campione, L. I. Basilio, L. K. Warne, and M. B. Sinclair, "Tailoring dielectric resonator geometries for directional scattering and Huygens' metasurfaces," *Optics Express,* vol. 23, pp. 2293-2307, 2015.

[4] M. Kerker, D. S. Wang, and C. L. Giles, "Electromagnetic scattering by magnetic spheres," *J. Opt. Soc. Am.,* vol. 73, pp. 765-767, 1983.

[5] J. M. Geffrin, B. García-Cámara, R. Gómez-Medina, P. Albella, L. S. Froufe-Pérez, C. Eyraud*, et al.*, "Magnetic and electric coherence in forward- and back-scattered electromagnetic waves by a single dielectric subwavelength sphere," *Nat Commun,* vol. 3, p. 1171, 11/06/online 2012.

[6] Y. H. Fu, A. I. Kuznetsov, A. E. Miroshnichenko, Y. F. Yu, and B. Luk/'yanchuk, "Directional visible light scattering by silicon nanoparticles," *Nat Commun,* vol. 4, p. 1527, 02/26/online 2013.

[7] M. Decker, I. Staude, M. Falkner, J. Dominguez, D. N. Neshev, I. Brener*, et al.*, "High-efficiency light-wave control with all-dielectric optical Huygens' metasurfaces," *arXiv:1405.5038,* 2014.

[8] C. Pfeiffer and A. Grbic, "Metamaterial Huygens' Surfaces: Tailoring Wave Fronts with Reflectionless Sheets," *Physical Review Letters,* vol. 110, p. 197401, 05/06/ 2013.

[9] K. E. Chong, I. Staude, A. James, J. Dominguez, S. Liu, S. Campione*, et al.*, "Polarization-Independent Silicon Metadevices for Efficient Optical Wavefront Control," *Nano Letters,* vol. 15, pp. 5369-5374, 2015/08/12 2015.

[10] A. Alu and N. Engheta, "Polarizabilities and effective parameters for collections of spherical nanoparticles formed by pairs of concentric double-negative, single-negative, and/or double-positive metamaterial layers (vol 97, pg 094310, 2005)," *Journal of Applied Physics,* vol. 99, Mar 2006.

[11] L. I. Basilio, L. K. Warne, W. L. Langston, W. A. Johnson, and M. B. Sinclair, "A Quick and Easy Simulation Procedure to Aid in Metamaterial Unit-Cell Design," *Antennas and Wireless Propagation Letters, IEEE,* vol. 10, pp. 1567-1570, 2011.

[12] C. Rockstuhl, C. Menzel, S. Mühlig, J. Petschulat, C. Helgert, C. Etrich*, et al.*, "Scattering properties of meta-atoms," *Physical Review B,* vol. 83, p. 245119, 06/23/ 2011.

[13] Y. Yang, I. I. Kravchenko, D. P. Briggs, and J. Valentine, "All-dielectric metasurface analogue of electromagnetically induced transparency," *Nat Commun,* vol. 5, 12/16/online 2014.

[14] W. Zhao, X. Leng, and Y. Jiang, "Fano resonance in all-dielectric binary nanodisk array realizing optical filter with efficient linewidth tuning," *Optics Express,* vol. 23, pp. 6858-6866, 2015/03/09 2015.

[15] F. Wang, Q.-H. Wei, and H. Htoon, "Switchable and non-switchable zero backscattering of dielectric nano-resonators," *Optical Materials Express,* vol. 5, pp. 668-675, 2015/03/01 2015.

[16] S. Tretyakov, *Analytical Modeling in Applied Electromagnetics*. London, UK: Artech House, 2003.